

## Effect of barite on the rheological properties of an oil-based drilling fluid

Titus Ntow Ofei<sup>1</sup>, Bjørnar Lund<sup>2\*</sup>, Knud Richard Gyland<sup>3</sup>, and Arild Saasen<sup>4</sup>

<sup>1</sup>Norwegian University of Science and Technology, Trondheim, Norway

<sup>2</sup>SINTEF, Trondheim, Norway

<sup>3</sup>M-I SWACO, Schlumberger Norge AS

<sup>4</sup>University of Stavanger, Stavanger, Norway

### ABSTRACT

Control of downhole pressure and transportation of cuttings to surface are two main tasks of a drilling fluid. While adequate pressure control is often obtained by increasing the density of the fluid by adding barite (or other similar high-density solids), these weight additives also affect rheological properties of the fluid. This in turn not only has consequences for the ability to transport cuttings but also impacts the downhole pressure as the frictional pressure loss will be changed. Thus, understanding the effect of barite concentration on the rheological properties is of significant industrial interest, while it also is a challenging scientific problem due to the complex structure of a drilling fluid.

In this paper we present results from an experimental investigation of the rheological properties of three samples of oil-based drilling fluids with densities of  $1430 \frac{kg}{m^3}$  (SG = 1.43),  $1550 \frac{kg}{m^3}$  (SG = 1.55) and  $1600 \frac{kg}{m^3}$  (SG = 1.60), respectively. The density was varied by varying the barite concentration, while the mass fraction of the other components was unchanged.

The rheological properties were characterized using a Couette type rheometer. Parameters for the Herschel-Bulkley model were generated from flow curves, while viscoelastic properties were investigated using oscillatory test.

We find that the effect of increasing barite concentration on yield stress is

significantly larger from  $1550 \frac{kg}{m^3}$  to  $1600 \frac{kg}{m^3}$  than from  $1430 \frac{kg}{m^3}$  to  $1550 \frac{kg}{m^3}$ . This is particularly important for the resistance to barite sag. The consistency index increases more gradually, while the flow behaviour index is not affected significantly. We discuss possible causes and implications of this observation.

### INTRODUCTION

Control of downhole pressure and transportation of cuttings to surface are two main tasks of a drilling fluid. Oil-based drilling fluids are frequently used as they do not react chemically with the formation rock. The viscosity of oil-based drilling fluids (OBDF) depends on several factors including type of liquid and solid additives and their interactions, pressure, and temperature. Viscosity of such complex liquids is the result of internal frictional forces between different layers, as they are forced to move relative to each other. These forces are caused by attractive and repulsive forces between the particles, droplets, and chemicals. When the temperature increases, the viscosity of liquids normally decreases, and when the pressure increases the viscosity normally increases. Hence, an increase both in pressure and temperature resulting from drilling deeper in a well, will lead to a change in viscosity that is strongly dependent on the drilling fluid composition.

The most common viscosity model for drilling fluids with a reasonable accuracy

over a wide span of shear rates is the Herschel-Bulkley model based on the observations by Herschel and Bulkley<sup>1</sup>. The Herschel-Bulkley fluid model combines a Power-law behaviour with a yield stress.

Oil-based drilling fluids typically contains 15-35% water in a dispersed brine phase, and thus referred to as invert-emulsion fluids. When considering the oil to water ratio (OWR) of oil-based drilling fluids, increase in water percentage leads to an increase in viscosity. Although oil is more viscous than water, the water droplets interact with the solid particles and some water droplets will have to move for others to come through. Consequently, the viscosity increases.

Barite, a mineral consisting of barium sulfate, is a solid material added to adjust the density of drilling fluids in order to keep the wellbore stable. Generally, added solid particles to the drilling fluid will increase the drilling fluid viscosity. Halvorsen et al.<sup>2</sup> found that little effect of barite addition was found on viscous parameters before reaching a sufficient barite concentration. For the oil to water ratio (OWR) investigated, no significant effect was observed on the yield stress before the density reached SG = 1.6. However, the general drilling fluid viscosity seems to have increased already from SG = 1.4. This is illustrated in Figure 1, which shows the Herschel-Bulkley parameters for dimension-less shear rates as function of drilling fluid density.<sup>3</sup> In the current paper we are looking in more detail into the effect of barite addition on the rheological properties of oil-based drilling fluids.

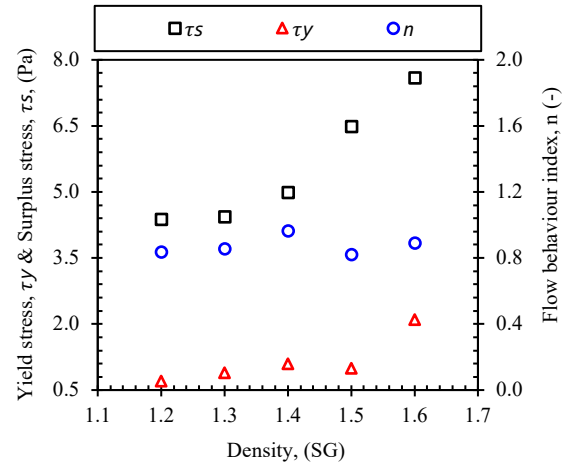


Figure 1. The effect of density on Herschel-Bulkley parameters,  $\tau_y$ ,  $\tau_s$ , and  $n$  (Halvorsen et al.<sup>2</sup>).

## MATERIALS AND METHOD

The experimental setup and procedures for characterizing the fluid samples as well as the fluid composition and mixing are the same as described in earlier publications by Ofei et al.<sup>4,5</sup>

### Fluid components

We formulated three different oil-based drilling fluid (OBDF) samples with the same oil-water ratio of 80/20 but different barite volume concentrations of 0.145, 0.181, and 0.196, corresponding to fluid densities of  $1430 \frac{kg}{m^3}$  (SG = 1.43),  $1550 \frac{kg}{m^3}$  (SG = 1.55), and  $1600 \frac{kg}{m^3}$  (SG = 1.60) respectively. The fluid components were supplied by M-I SWACO, Schlumberger, Norge AS, and consisted of a refined mineral oil as a base fluid of density  $814 \frac{kg}{m^3}$  and kinematic viscosity of  $5.9 \frac{mm^2}{s}$ , brine of calcium chloride, lime, emulsifier, organophilic clay viscosifiers, fluid loss agent, low gravity calcium carbonate, and API grade barite. A spindle mixer was used to mix the components of the drilling fluid at a speed of 6000 rpm for a total of 70 minutes. Table 1 shows the mixing order and mass

concentration of the various components of the drilling fluids.

Table 1. Composition of 1L fluid samples for different specific gravity (SG)

| Mixing order | Product (OWR = 80/20)            | SG=1.43 (g/L) | SG=1.55 (g/L) | SG=1.60 (g/L) |
|--------------|----------------------------------|---------------|---------------|---------------|
| 1            | Refined mineral oil (base fluid) | 501.9         | 473.8         | 463.0         |
| 2            | Emulsifier                       | 20.0          | 21.6          | 22.3          |
| 3            | Viscosifier (low temp. clay)     | 9.0           | 9.7           | 10.0          |
| 4            | Viscosifier (high temp. clay)    | 13.0          | 14.0          | 14.5          |
| 5            | Lime                             | 20.0          | 21.6          | 22.3          |
| 6            | Fluid loss agent                 | 10.0          | 10.8          | 11.2          |
| 7            | Calcium chloride brine           | 199.3         | 183.5         | 179.3         |
| 8            | API grade barite                 | 610.0         | 760.9         | 821.6         |
| 9            | Calcium carbonate (low gravity)  | 50.0          | 54.0          | 55.8          |

### Fluid mixing procedure

In preparation of the drilling fluid, the following procedure was used for mixing. The drilling fluid components, concentration and mixing procedure were recommended by the supplier.

- Pour the refined mineral oil in a container and place the container in ice water bath to maintain the fluid's temperature below 65°C. The use of a cooling bath is not necessary until the temperature exceeds 55°C. It should be noted that some of the components require initial heating to better dissolve in the base oil and to be fully activated.
- Pour the base oil into a spindle mixer container and add the emulsifier and mix for 2 minutes.
- Add the low temperature and high temperature viscosifiers to the mixing container and mix for 8 minutes.
- Afterwards, add the lime to the container and mix for 5 minutes.
- Add the fluid loss agent and mix for 5 minutes.
- Add the brine of calcium chloride and mix for 15 minutes.
- Add the barite and mix for 25 minutes.
- Finally, add the calcium carbonate to the mixture and mix for 10 minutes to act as a bridging material which reduces fluid loss and minimizes filter cake thickness, especially in permeable formation.

### Particle size distribution

The particle size distribution of the API grade barite for specific gravity (SG) in the range of 4.1-4.2 was characterized using a light scattering (LS) particle size analyzer. The instrument uses laser light with a wavelength of 750 nm to measure the size of particles with diameters from 0.04  $\mu\text{m}$  to 2000  $\mu\text{m}$  by light diffraction. The laser's radiation passes through a spatial filter and projection lens to form a beam of light. The beam passes through the sample cell where particles suspended in liquid or air scatter the incident light in characteristic patterns which depends on their sizes. Figure 2 shows the particle size distribution (PSD) of the API barite with  $D_{10}$ ,  $D_{50}$  and  $D_{90}$  values as 0.658  $\mu\text{m}$ , 6.909  $\mu\text{m}$ , and 34.130  $\mu\text{m}$  respectively. The  $D_x$  value indicates that  $x$  % of the particles by mass have diameters that are smaller than this value.

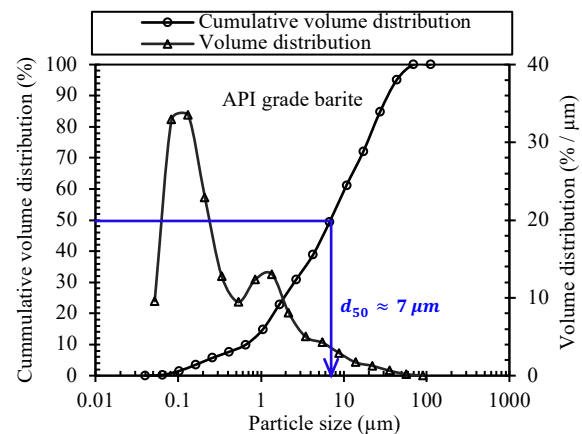


Figure 2. Particle size distribution of API grade barite.

### Rotational rheometry test

An Anton Paar rheometer (*MCR 302*) using a Couette geometry with a grooved bob was utilized to conduct the rheological measurements on the OBDF at 25°C. The various rheological tests performed include flow curves, oscillatory amplitude sweep, oscillatory frequency sweep, and tests at constant rotational and oscillatory shear rates.

The flow curves were measured under controlled shear rates and show the shear stress versus shear rate of the sample. We pre-sheared the sample at a constant shear rate of  $1022 \text{ s}^{-1}$  for 300 s before linearly ramping down the shear rate from 1022 to  $1.0 \text{ s}^{-1}$  for 100 measuring points with a 5 s measuring duration per point. Then, the shear rate was logarithmically ramped down from  $1.0 \text{ s}^{-1}$  to  $0.001 \text{ s}^{-1}$  for 40 measuring points with a 4 s measuring duration per point to capture the flow characteristics in the ultralow shear rate region. In a similar manner, the shear rate was ramped up logarithmically from  $0.001 \text{ s}^{-1}$  to  $1.0 \text{ s}^{-1}$  for 40 measuring points with 4 s measuring point duration and then linearly ramped up from  $1.0 \text{ s}^{-1}$  to  $1022 \text{ s}^{-1}$  for a total of 100 measuring points with 5 s measuring point duration. A difference between the ramping down and ramping up flow curves indicates the thixotropy of the fluid sample.<sup>6,7</sup> The present study reveals insignificant differences between the flow curves.

By performing oscillatory shear tests, certain parameters have been adopted from continuum mechanics to measure the rheological properties of the viscoelastic fluid. The shear modulus  $G$ , under uniaxial stress conditions, according to Hooke's law, is constant for perfectly elastic material. However, for oscillatory stresses, a complex shear modulus,  $G^*$ , which is divided into a storage modulus,  $G'$ , and a loss modulus,  $G''$ , is defined as follows<sup>8</sup>:

$$G^* = \frac{\tau_A}{\gamma_A} \quad (1)$$

$$G' = |G^*| \cos(\delta) = \left| \frac{\tau_A}{\gamma_A} \right| \cos(\delta) \quad (2)$$

$$G'' = |G^*| \sin(\delta) = \left| \frac{\tau_A}{\gamma_A} \right| \sin(\delta) \quad (3)$$

where  $\tau_A$  is the complex stress amplitude,  $\gamma_A$  is the corresponding complex strain

amplitude, and  $\delta$  is the phase shift angle between  $\tau_A$  and  $\gamma_A$ .

The amplitude sweep tests which use sinusoidal oscillations allow the testing of the microstructure of the sample without breaking the sample structure.<sup>9</sup> The test was carried out with a constant angular frequency of  $10 \frac{\text{rad}}{\text{s}}$  and increasing strain amplitude from 0.001 to 100 % at a slope of 5 measuring points per decimal, accounting to 26 measuring points. The limit of the linear viscoelastic (LVE) range, below which the microstructure of the sample is intact, is determined for use as a parameter for the frequency sweep test at a tolerance limit of 97 %. The test also measures the storage modulus ( $G'$ ), characterizing the material's elastic behavior, and loss modulus ( $G''$ ), characterizing the viscous behavior of the material, both as function of the strain amplitude. The flow point, where  $G' = G''$ , is determined as the point where the material's microstructure is destroyed, and flow is initiated. In regions where  $G' > G''$  the elastic behavior dominates the viscous behavior and the sample depicts a solid-like character. Conversely,  $G'' > G'$ , indicates that the viscous behavior dominates the elastic behavior of the sample and shows a liquid-like character.

A frequency sweep test uses sinusoidal oscillations at small strain amplitudes usually within the LVE region.<sup>9</sup> Here a shear strain amplitude within the LVE region was applied on the sample over a range of decreasing angular frequency from 100 to  $0.001 \frac{\text{rad}}{\text{s}}$  at a slope of 5 measuring points per decimal, amounting to 26 measuring points. The phase shift angle  $\delta$ , which is indicative of ideal solid behaviour at  $0^\circ$  and purely liquid behaviour at  $90^\circ$ , is measured to evaluate the viscoelastic behaviour of the fluid sample. The viscoelastic behaviour is often expressed in terms of the damping factor  $\tan(\delta) = \frac{G''}{G'}$  which indicates whether the sample is more viscous when  $\tan(\delta) >$

1, or more elastic when  $\tan(\delta) < 1$ . It also defines the gel property of the fluid sample.<sup>10</sup>

*Herschel-Bulkley model parameters*

The Herschel-Bulkley model is a three-parameter model which is known to describe well the flow characteristics of most non-Newtonian drilling fluids. Here, we present three different approaches, namely, traditional, Saasen-Ytrehus, and Kelessidis, for calculating the model parameters: the flow behaviour index,  $n$ , the consistency index,  $K$ , and the yield stress,  $\tau_y$ . As measurement techniques for yield stress are more sensitive, we first determine the yield stress value and then fit the other parameters.

*Traditional approach*

The traditional approach expresses the Herschel-Bulkley model in terms of the parameters  $n$ ,  $K$ , and  $\tau_y$  as:

$$\tau(\dot{\gamma}) = \tau_y + K\dot{\gamma}^n \quad (4)$$

where  $\dot{\gamma}$  is the shear rate.

The yield stress,  $\tau_y$ , value is estimated by extrapolation from the low shear measurements down to zero shear rate. Unless stated otherwise, the extrapolation is linear from the two lowest shear rate values. We then determine  $n$  and  $K$  by a least-square regression of the linearized form of Eq. 4 as:

$$\ln(\tau - \tau_y) = \ln(K) + n\ln(\dot{\gamma}) \quad (5)$$

The parameters are measured for shear rates below a maximum shear rate,  $\dot{\gamma}_{\max}$ , corresponding to the highest expected shear rate in the application to be considered.

*Saasen-Ytrehus approach*

This approach presented by Saasen and Ytrehus<sup>3</sup> was based on a representation by Nelson and Ewoldt<sup>11</sup> for describing drilling

fluids in accordance with the API or ISO specifications. They<sup>3</sup> noted that the traditional Herschel-Bulkley consistency index,  $K$ , is dimensionally dependent on the flow behaviour index,  $n$ , thereby hindering optimum digitalization process within the drilling industry. They presented the following representation:

$$\tau(\dot{\gamma}) = \tau_y + \tau_s \left( \frac{\dot{\gamma}}{\dot{\gamma}_s} \right)^n \quad (6)$$

The surplus stress is determined as  $\tau_s = \tau(\dot{\gamma}_s) - \tau_y$  where  $\tau(\dot{\gamma}_s)$  is the measured shear stress at a predetermined shear rate  $\dot{\gamma}_s$  which is characteristic of the flow process to be modelled. The yield stress,  $\tau_y$ , is determined first, using the same approach as in the traditional approach.

The flow behaviour index,  $n$ , is then determined by matching Eq. (6) to the measured shear stress  $\tau_x$  at a selected shear rate  $\dot{\gamma}_x$ . Solving for  $n$ , we then obtain:

$$n = \frac{\ln\left(\frac{\tau_x - \tau_y}{\tau_s}\right)}{\ln\left(\frac{\dot{\gamma}_x}{\dot{\gamma}_s}\right)} \quad (7)$$

The shear rates,  $\dot{\gamma}_x$  and  $\dot{\gamma}_s$ , should be within the relevant shear rate range for the flow problem to be evaluated. In this study, we have used  $\dot{\gamma}_x = 100 \text{ s}^{-1}$  and  $\dot{\gamma}_s = 300 \text{ s}^{-1}$ .

The consistency index,  $K$ , can then be calculated from:

$$\tau_s = K\dot{\gamma}_s^n \quad (8)$$

*Kelessidis approach*

This approach<sup>12</sup> is similar to the traditional approach, but instead of determining the yield stress by extrapolation, it is determined by maximizing the coefficient of determination,  $R^2$ , defined as:

$$R^2 = 1 - \frac{\sum_i (y_i - f_i)^2}{\sum_i (y_i - \bar{y})^2} \quad (9)$$

where  $y_i$  is measurement or observation  $i$  (in this case shear stress),  $f_i$  is the corresponding modelled value, and  $\bar{y}$  is the mean value of the observed data.

For each value of  $\tau_y$ , the parameters  $K$  and  $n$  are determined by least square fitting of the linearized equation (5).

We use a slightly modified version of the Kelessidis representation as follows:

- a) For each value of  $\tau_y$ , the parameters  $K$  and  $n$  are determined by least square fitting of the nonlinear equation (4). We also note that Eq. (5) is not mathematically correct since it is not permissible to take the logarithm of a dimensional quantity.
- b) Since the numerator does not depend on the parameters to be fitted, we instead minimize the error norm using:

$$S_2 = \frac{\sum_i (y_i - f_i)^2}{N} \quad (10)$$

Or the corresponding normalized error norm using:

$$S_{2n} = \frac{\sum_i \left( \frac{y_i - f_i}{y_i} \right)^2}{N} \quad (11)$$

where,  $N$ , is the number of measurement points.

The latter error norm (Eq. 11) gives more weight to the low shear data. While  $S_2$  is associated with  $R^2$ , we associate  $S_{2n}$  with:

$$R^{2n} \equiv 1 - \frac{\sum_i \left( \frac{y_i - f_i}{y_i} \right)^2}{\sum_i \left( \frac{y_i - \bar{y}}{\bar{y}} \right)^2} \quad (12)$$

## RESULTS AND DISCUSSION

### Viscosity flow curves

Figure 3 presents the rheometry measurements of three oil-based drilling fluid (OBDF) samples with different barite concentrations. All the viscosity profiles show shear thinning behaviour over the range of shear rates, at least below  $200 \text{ s}^{-1}$ . They also show a consistently increasing dynamic viscosity with increasing barite concentration. This increase is very dramatic especially at low shear rates. It is also noted that the flow curve is fairly linear above  $200 \text{ s}^{-1}$ .

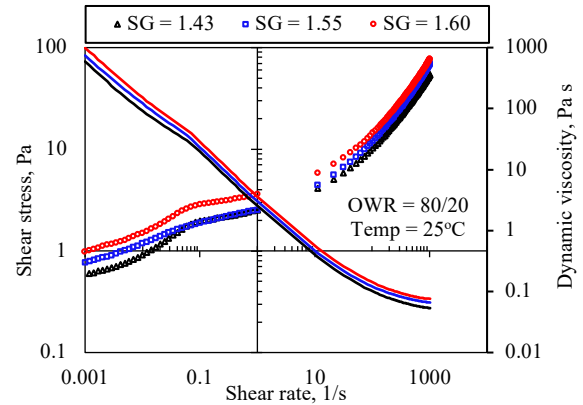


Figure 3. Viscosity flow curves of OBDF samples with different barite concentrations.

### Model comparison

The model flow curves are compared with the experimental measurements as shown in Figures 4, 5, and 6, corresponding to fluid sample densities of  $\text{SG} = 1.43$ ,  $\text{SG} = 1.55$ , and  $\text{SG} = 1.60$ , respectively. We have selected data below a shear rate of  $300 \text{ s}^{-1}$ . This is in relation to shear rates usually experienced in the field, except for the flow around the Bottom Hole Assembly (BHA).<sup>13,14</sup> It is noted that at very low shear rates the Herschel-Bulkley model gives a poor fit. Also, the measured shear stresses do not converge to a constant value at low shear rates. However, both the Traditional and Saasen-Ytrehus approaches by design closely match the measured data at  $0.001 \text{ s}^{-1}$ .

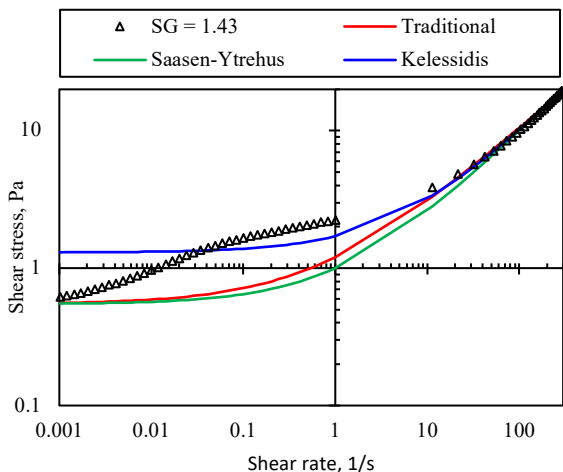


Figure 4. Comparing measurements with different representations of the Herschel-Bulkley model fit for  $SG = 1.43$ .

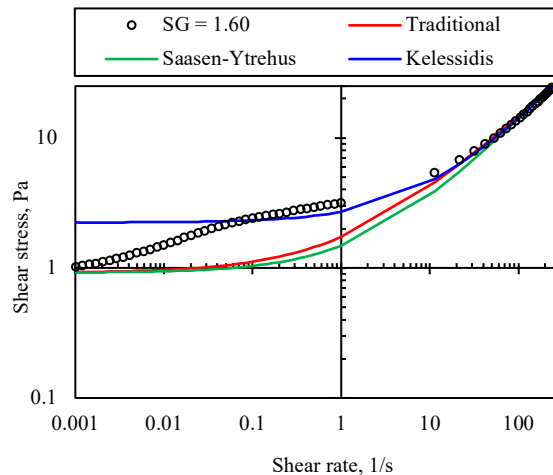


Figure 6. Comparing measurements with different representations of the Herschel-Bulkley model fit for  $SG = 1.60$ .

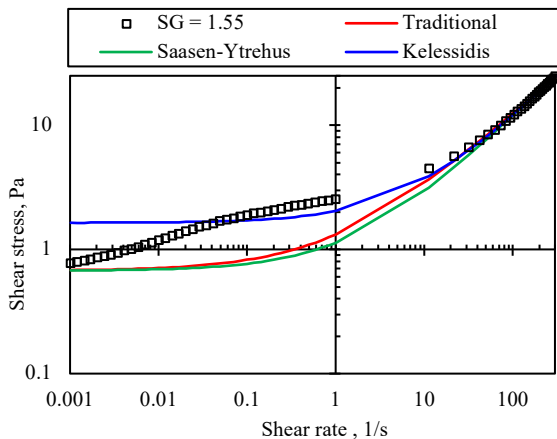


Figure 5. Comparing measurements with different representations of the Herschel-Bulkley model fit for  $SG = 1.55$ .

*Effect of barite concentration on Herschel-Bulkley parameters*

From the viscosity flow curve in Figure 3, there does not appear to be any converged yield stress. However, using the Saasen-Ytrehus approach, the extracted yield stress,  $\tau_y$ , increases with barite concentration, as shown in Figure 7. The consistency index,  $K$ , and the surplus stress,  $\tau_s$ , also increase with barite concentration, while the flow behaviour index,  $n$  is essentially unaffected. The latter is similar to the observation by Chateau et al.<sup>15</sup> However, we note that, the authors assumed the system was composed of a suspension of noncolloidal and non-Brownian particles in a nonlinear fluid with experimental validation for monodisperse particles. Here, we have a polydisperse system, where the smallest particles are in the sub-micrometer range.

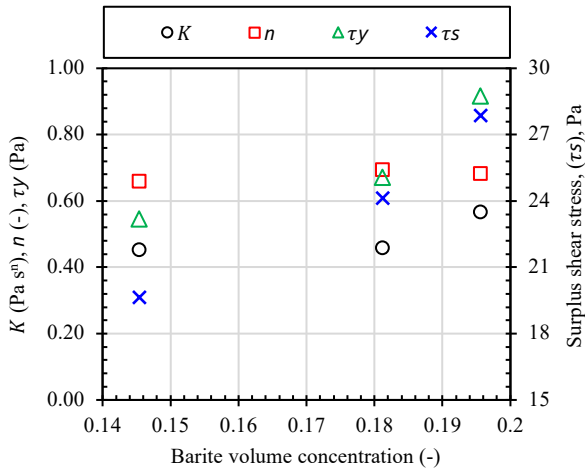


Figure 7. Dependency of Herschel-Bulkley parameters on the barite volume concentration.

Figure 8 compares the effect of barite concentration on yield stress using the three approaches. It is observed that the Kelessidis model estimated more than twice as high yield stress values for different barite volume concentrations. It should be noted that both the traditional and the Saasen-Ytrehus approaches predicted the same yield stress values because both approaches used the same method for determining the yield stress values.

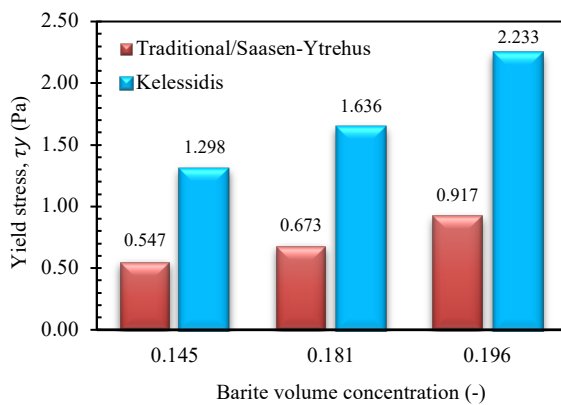


Figure 8. Model comparison of yield stress parameters for different barite volume concentration.

The effect of barite concentration on the Herschel-Bulkley parameters: consistency index,  $K$ , and flow behaviour index,  $n$ , are presented in Figure 9 and 10, respectively. It

is evident that as barite concentration increase in the fluid samples, there is a gradual increase in the  $K$  values as estimated from all the approaches as shown in Figure 9. This is due to the increase of cohesive forces between the particles, droplets, and chemicals. The Traditional approach, however, estimated higher  $K$  values compared to the Saasen-Ytrehus and Kelessidis approaches. On the contrary, the flow behaviour index,  $n$ , values did not change significantly as the barite concentration increased as estimated by all the approaches, as was also observed by Halvorsen et al.<sup>2</sup> The Kelessidis approach slightly predicted higher  $n$  values than the traditional and Saasen-Ytrehus approaches.

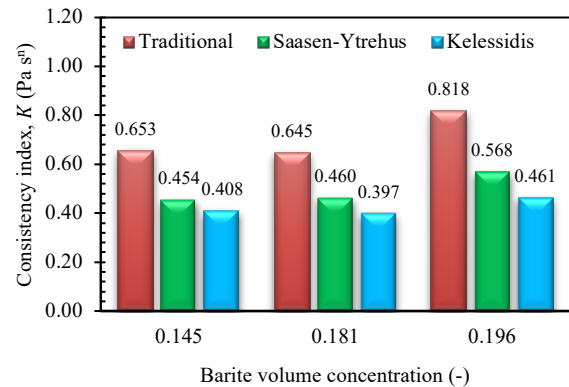


Figure 9. Model comparison of consistency index parameters for different barite volume concentration.

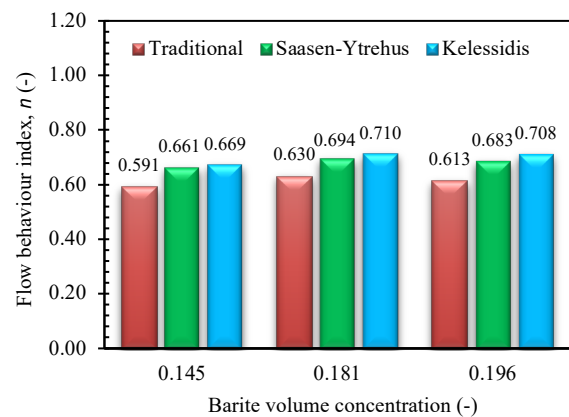


Figure 10. Model comparison of flow behaviour parameters for different barite volume concentration.

Tables 2 to 4 show the estimated Herschel-Bulkley model parameters with their error norms.

Table 2. Herschel-Bulkley parameters and error norms  $R^2$  and  $R^{2n}$  calculated using flow data with SG = 1.43.

| Model          | $K$ [Pas <sup>n</sup> ] | $n$ [-] | $\tau_y$ [Pa] | $\tau_s$ [Pa] | $R^2$   | $R^{2n}$ |
|----------------|-------------------------|---------|---------------|---------------|---------|----------|
| Traditional    | 0.65334                 | 0.59102 | 0.54733       |               | 0.99136 | 0.8913   |
| Saasen-Ytrehus | 0.45357                 | 0.66076 | 0.54733       | 19.6527       | 0.98992 | 0.87043  |
| Kelessidis     | 0.40798                 | 0.66947 | 1.2981        |               | 0.99702 | 0.87223  |

Table 3. Herschel-Bulkley parameters and error norms  $R^2$  and  $R^{2n}$  calculated using flow data with SG = 1.55.

| Model          | $K$ [Pas <sup>n</sup> ] | $n$ [-] | $\tau_y$ [Pa] | $\tau_s$ [Pa] | $R^2$   | $R^{2n}$ |
|----------------|-------------------------|---------|---------------|---------------|---------|----------|
| Traditional    | 0.64468                 | 0.62979 | 0.673         |               | 0.99236 | 0.89259  |
| Saasen-Ytrehus | 0.45993                 | 0.69428 | 0.673         | 24.127        | 0.99118 | 0.87696  |
| Kelessidis     | 0.39709                 | 0.71008 | 1.6364        |               | 0.99741 | 0.87555  |

Table 4. Herschel-Bulkley parameters and error norms  $R^2$  and  $R^{2n}$  calculated using flow data with SG = 1.60.

| Model          | $K$ [Pas <sup>n</sup> ] | $n$ [-] | $\tau_y$ [Pa] | $\tau_s$ [Pa] | $R^2$   | $R^{2n}$ |
|----------------|-------------------------|---------|---------------|---------------|---------|----------|
| Traditional    | 0.81755                 | 0.6129  | 0.91667       |               | 0.99184 | 0.90151  |
| Saasen-Ytrehus | 0.56754                 | 0.68279 | 0.91667       | 27.8833       | 0.99041 | 0.88458  |
| Kelessidis     | 0.46085                 | 0.7079  | 2.233         |               | 0.99665 | 0.84366  |

*Dynamic yield stress*

The dynamic yield stress,  $\tau_{dy}$ , refers to a quantity measured under dynamic conditions where a constant or time-varying shear rate is applied. This value is estimated more accurately from the amplitude sweep test where the yield stress of the material is determined as the stress where  $G' = 0.9G'_{linear}$ . Figure 11 shows the  $\tau_{dy}$  values for the three fluid samples where the  $\tau_{dy}$  values increases as the densities of the fluid samples increase. The  $\tau_{dy}$  values recorded in Figure 8 are 0.406 Pa, 0.660 Pa, and 0.814 Pa, corresponding to SG = 1.43, SG = 1.55, and SG = 1.60, respectively. These values are very close to the yield stress,  $\tau_y$ , values predicted by the traditional and Saasen-Ytrehus approaches, while the

Kelessidis approach gave higher values, as shown in Figure 8.

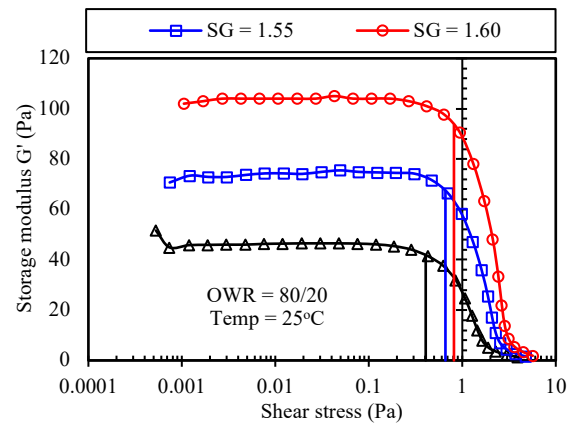


Figure 11. Storage modulus vs shear stress for three different fluid densities. The dynamic yield stress,  $\tau_{dy}$ , values are determined at  $G' = 0.9G'_{linear}$ , marked by vertical lines.

CONCLUSIONS

In this paper, we presented experimental investigation of the effect of barite concentration on the Herschel-Bulkley rheological parameters of oil-based drilling fluids. The Herschel-Bulkley parameters were estimated using three approaches: traditional, Saasen-Ytrehus, and Kelessidis. The following could be inferred:

1. An increase in barite concentration increases the yield stress and the consistency index of the fluid samples, while the flow behaviour index is not significantly affected.
2. The dynamic yield stress values measured from the amplitude sweep test closely matched the yield stress values estimated from the Traditional and the Saasen-Ytrehus approaches.
3. The Kelessidis approach produced twice as high yield stress values and lower consistency index values than the Traditional and the Saasen-Ytrehus approaches. However, the estimation of the flow behaviour index parameters is fairly similar for all three approaches.

## ACKNOWLEDGMENTS

This work was carried out at the laboratories of NTNU and SINTEF in Norway. The authors acknowledge the financial support of the Research Council of Norway and the National Science Foundation of USA under Award Number 1743794 for the PIRE project "Multi-scale, Multiphase Phenomena in Complex Fluids for the Energy Industries". Special thanks to M-I SWACO, Schlumberger Norge AS for supplying the drilling fluid chemicals and providing technical support.

## REFERENCES

1. Herschel W.H. & Bulkley R. 1926. "Konsistenz-messungen von Gummibenzöllösungen", *Kolloid Z.* **39**, 291-300.
2. Halvorsen, H., Blikra, H.J., Grelland, S.S., Saasen, A. & Khalifeh, M. 2019. "Viscosity of Oil-Based Drilling Fluids", *Ann. Trans. Nordic Rheol. Soc.*, **27**, 77-85.
3. Saasen, A. & Ytrehus, J.D. 2018. "Rheological Properties of Drilling Fluids – Use of Dimensionless Shear Rates in Herschel-Bulkley Models and Power-Law Models", *Applied Rheology*, **28** (5), paper 54515. DOI: 10.3933/ApplRheol-28-54515.
4. Ofei, T.N., Lund, B., Saasen, A., Sangesland, S., Gyland, K.R., and Linga, H. 2019. "A New Approach to Dynamic Barite Sag Analysis on Typical Field Oil-Based Drilling Fluid", *Ann. Trans. Nordic Rheol. Soc.*, **27**, 61-69.
5. Ofei, T. N., Lund, B., Saasen, A., Sangesland, S., Linga, H., Gyland, K. R., & Kawaji, M. 2020. Barite Sag Measurements. Presented at the IADC/SPE International Drilling Conference and Exhibition, Galveston, Texas, USA, 3 – 5 March. SPE 199567-MS. <http://doi:10.2118/199567-MS>.
6. Cayeux, E. 2020. Time, Pressure and Temperature Dependent Rheological Properties of Drilling Fluids and Their Automatic Measurements. Presented at the IADC/SPE International Drilling Conference and Exhibition, Galveston, Texas, USA, 3 - 5 March. SPE 199641-MS.
7. Jachnik, R. 2005. "Drilling Fluid Thixotropy & Relevance", *Ann. Trans. Nordic Rheol. Soc.*, **13**, 1-6.
8. Mezger, T.G. 2014. *The Rheology Handbook*. 4ed. Vincentz Network, Hannover, Germany.
9. Savari, S., Kulkarni, S., Maxey, J., and Teke, K. 2013. "A Comprehensive Approach to Barite Sag Analysis on Field Muds", *AADE National Technical Conference and Exhibition*, Cox Convention Centre, Oklahoma City, February 26-27.
10. Saasen A., Liu, D., Marken, C.D., Sterri, N., Halsey, G.W., and Isambourg, P. 1995. "Prediction of Barite Sag Potential of Drilling Fluids from Rheological Measurements", SPE/IADC Number 29410, Presented at the SPE/IADC Drilling Conference, Amsterdam, 28 February – 2 March.
11. Nelson A.Z, Ewoldt R.H. 2017. "Design of Yield Stress Fluids: A Rheology-to-Structure Inverse Problem", *Soft Matter*, **13**, 7578-7594
12. Kelessidis, V. C., Maglione, R., Tsamantaki, C., and Aspirtakis, Y. 2006. "Optimal Determination of Rheological Parameters for Herschel–Bulkley Drilling Fluids and Impact on Pressure Drop, Velocity Profiles and Penetration Rates During Drilling," *J. Petrol Sci and Eng.*, **53** (3), pp. 203-224.
13. Sayindla, S., Lund, B., Ytrehus, J.D., and Saasen, A. 2017. "Hole-Cleaning Performance Comparison of Oil-Based and Water-Based Drilling Fluids". *J. Petrol. Sci. Eng.*, **159**, 49-57.
14. Werner, B., Myrseth, V., and Saasen, A. 2017. "Viscoelasticity Properties of Drilling Fluids and Their Influence on Cuttings Transport". *J. Petrol. Sci. Eng.*, **156**, 845-851.
15. Chateau, X., Ovarlez, G., and Trung, K. L. 2008. "Homogenization Approach to the Behavior of Suspensions of Noncolloidal Particles in Yield Stress Fluids," *J Rheol*, **52** (2), 489-506.